Astroparticle Physics 34 (2010) 70–79

Contents lists available at ScienceDirect

Astroparticle Physics

journal homepage: www.elsevier.com/locate/astropart

Radioactive background in a cryogenic dark matter experiment

V. Tomasello *, M. Robinson, V.A. Kudryavtsev

Department of Physics and Astronomy, University of Sheffield, Hounsfield Road, Sheffield S3 7RH, UK

ARTICLE INFO

Article history:
Received 22 October 2009
Received in revised form 7 April 2010
Accepted 24 May 2010
Available online 1 June 2010

Keywords:
Radioactivity
Neutron background
Gamma-ray background
Dark matter
WIMPs
Monte Carlo simulations

ABSTRACT

New generation dark matter experiments aim at exploring the $10^{-9} - 10^{-10}$ pb cross-section region for WIMP-nucleon scalar interactions. Neutrons and gamma-rays, due to radioactive processes, are produced in the detector components and are one of the main factors that can limit detector sensitivity. Estimation of the background from this source then becomes a crucial task for designing future large-scale detectors. Radioactive background event rates from some detector components (such as copper and stainless steel), as well as from rock and concrete (lab walls), were estimated in this work for a hypothetical cryogenic dark matter detector (for instance EURECA) with a target mass of 100–1000 kg. Different shielding configurations (water, lead, polyethylene, plexiglass) were considered. Neutrons and photons were propagated to the detector using GEANT4. Some requirements for the radio-purity of the materials were deduced from the results of these simulations. Thickness of shielding in different configurations and the required gamma discrimination factor were investigated.

1. Introduction

Theories beyond the Standard Model, such as Supersymmetry (SUSY), provide good candidates for the non-baryonic dark matter in the Universe, for instance WIMPs or Weakly Interacting Massive Particles. The direct detection of such particles is based on observation of their elastic scattering (nuclear recoil) on a suitable laboratory target. Small nuclear recoil energy E_r ($E_r \lesssim 100$ keV) and very low probability (between 1 and $\ll$1 event/kg/day) characterise the interaction, therefore a very low rate of background events can be tolerated. This requires an underground laboratory (depth of 3 km w.e. or more) and strict monitoring of any possible source of radiation. Such laboratories are capable of screening a detector from more conventional signals induced by cosmic rays (the layers of rock reduce their flux by a factor of 10^5–10^7 with respect to the surface). Theoretical predictions and experimental evidences suggest the 10^{-9}–10^{-10} pb region as the probable one for the WIMP-proton cross-section [1]. Reaching such a level of sensitivity requires a tonne-scale mass for the detector and at the same time radio-purity requirements become more constraining.

Detector design studies require careful treatment of all kinds of background. Extensive simulation work can help in evaluating background suppression and rejection strategies, requirements on the depth, amount of passive shielding, purity of materials, veto efficiency etc. for a given experiment. High-Z material and low-A material are known to be efficient in suppressing gamma-ray and neutron backgrounds respectively. Many factors can influence the selection of appropriate materials for construction, most important are contamination, availability and cost.

The goal of this paper is to outline requisites for a dark matter experimental set-up, that can significantly reduce radioactive background coming from laboratory walls, shielding and some detector components.

Alphas, electrons/positrons, gamma-rays (X-rays) and neutrons are the kinds of particles that may be present among the radioactive decay products. Alphas and electrons, because of their very short range (few microns and few millimetres respectively) due to ionisation energy loss, need to be produced very close to the detector fiducial volume to generate visible effects. Neutrons and gamma-rays can reach a dark matter detector from a large distance producing low-energy nuclear or electron recoils, respectively. High-energy electrons can produce bremsstrahlung photons with sufficient energy to reach the detector.

Gamma-rays can be suppressed using passive shielding or rejected by special identification tools. Gamma-ray flux from radioactivity usually exceeds by several orders of magnitude the neutron flux. However, gamma-rays generate electron recoils (e-recoils) in dark matter detectors that can be relatively easily discriminated from nuclear recoils (n-recoils) expected from WIMPs. Typical discrimination factors achieved in advanced dark matter detectors are of the order of 10^3–10^5 (see for instance, [2–5]), i.e. only one electron recoil out of 10^3–10^5 survives the discrimination cuts without significant loss of nuclear recoil events. For any future dark matter detector aiming at probing the region of parameter space favoured by SUSY models (down to 10^{-10} pb) the gamma-

* Corresponding author. Tel.: +44 114 22 23553; fax: +44 114 22 23555.
E-mail address: vitotomasello@gmail.com (V. Tomasello).

0927-6505/$ - see front matter © 2010 Elsevier B.V. All rights reserved.
doi:10.1016/j.astropartphys.2010.05.005

induced background should not exceed the discrimination factor reducing the number of background events due to gamma interactions passing all cuts to less than one for the whole period of observations.

Neutron background can be attenuated by the use of passive shielding. Its suppression is essential, because neutron interaction with the target can give the same signal as the one expected from WIMPs. Some fraction of neutrons can be rejected using coincidence with an active veto system if positioned just around the target. The efficiency of such rejection in realistic conditions is not high, however, due to the difficulty in building a low-threshold veto system surrounding the target from all sides, that would not introduce any additional background in the detector itself [6]. In future large-scale experiments, neutrons from radioactivity in detector components may become a factor that limits the sensitivity of the detector.

Background studies for a large-scale detector can be found in Ref. [7] for a xenon target. In the present paper, for the first time, a large cryogenic detector with Ge crystals as the target was modelled. We estimated event rates from some possible radioactive sources in the experimental set-up. The following materials were examined as sources of background radiation: rock, concrete, lead, polyethylene, plexiglass, copper, stainless steel.

Simulations presented in this paper aim to investigate possible design solutions for EURECA (European Underground Rare Event Calorimeter Array) [8]. The EURECA collaboration focusses on cryogenic dark matter search in Europe. It is composed of the CRESST, EDELWEISS and ROSEBUD experimental groups and other institutes and scientists, that have joined the collaboration in recent years. EURECA will use a target mass of up to one tonne to explore WIMP-nucleon scalar scattering cross-section in the region of 10^{-9}–10^{-10} pb. A major advantage of EURECA is the planned use of more than one target material (multi-target experiment for WIMP identification). The ability to test the A-scaling of the WIMP-nucleon scattering cross-section will be an important tool for confirming the signal as being a positive evidence for WIMP interactions, also reducing systematic errors. Here we concentrated mainly on germanium crystals, other candidate targets for EURECA are $CaWO_4$ and other solid state scintillators.

The Laboratoire Souterrain de Modane (LSM) has been selected as a host laboratory for EURECA. The design of the experiment and a new underground laboratory hall to host it are not finalised yet. These simulations are contributing to the design of this new cryogenic dark matter experiment EURECA, its infrastructure and the new laboratory hall.

An outline of radioactive background simulations for 100 kg target is presented in Section 2. Simulations and results are described in two separate sections depending on the background source considered: Section 3 – for laboratory walls and Section 4 – for shielding and detector components. First simulations for a tonne-scale target mass are presented in Section 5.

2. Simulations of background from radioactivity

Background from radioactivity imposes severe constraints on the sensitivity of detectors and dominates over the cosmic-ray induced background at a depth of 3 km w.e. by three orders of magnitude. Background comes from U/Th decay chains, as well as from the decays of ^{40}K, ^{60}Co and some other long and short-lived isotopes. Passive shielding and active rejection techniques (*e*-recoil discrimination) provide further suppression of gamma background, however neutrons are more penetrating and more dangerous: a single nuclear recoil from neutron elastic scattering cannot be distinguished from the predicted WIMP-signal. Hence, neutron background must be well understood. Monte Carlo simulations are a valid investigative tool for this purpose.

In our simulations neutrons associated with local radioactivity were produced via spontaneous fission of U and (α,n) reactions initiated by α-particles from U/Th traces in the rock and detector components. Gamma-rays were produced by U/Th decay chains and ^{40}K. Decay chains were assumed to be in secular equilibrium.

Rates and spectra for gamma-ray production do not depend on the material for a fixed radioisotope concentration and are available from databases. They can also be generated with GEANT4 [9], as was done in Ref. [10] and used here. Neutron spectra depend on the material even for fixed radioisotope concentration because of the material-dependent cross-section of (α,n) reactions and branching ratios for transitions to excited states. This makes the neutron flux calculation more difficult compared to gamma-rays. The measurements of neutron fluxes and spectra in various materials are not straightforward either. The neutron spectra have to be evaluated for all materials relevant to dark matter searches. Neutron yields and spectra were calculated in this work, as described in Ref. [11], using a modified version of SOURCES4A [12,7,13]. EMPIRE2.19 [14] was used to calculate (α,n) cross-sections and

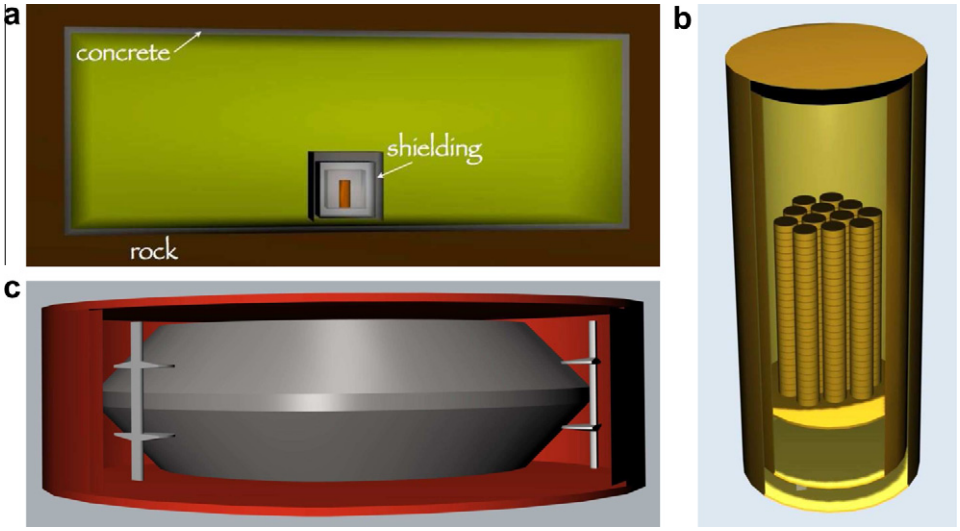

Fig. 1. Schematic view of the experimental hall of the underground lab (a), cryostat (b) and crystal (c) from GEANT4.

Table 1
Compositions of rock and concrete at LSM in % of mass (rock density = 2.65 g/cm^3, concrete density = 2.4 g/cm^3).

Element	H	C	O	Na	Mg	Al	Si	P	K	Ca	Ti	Mn	Fe
Rock	1	5.94	49.4	0.44	0.84	2.58	6.93	0.06	0.21	30.6	0.07	0.03	1.9
Concrete	1.09	7.78	49.68	0.01	0.78	0.48	2.69	0.07	0.02	36.78	0.09	0.01	0.52

branching ratio for transitions to excited states. These data were then added to the library of SOURCES4A. This was done for most of the materials used in detector construction. Primary particles (neutrons and gammas) were generated as evenly distributed in the source and emitted isotropically.

GEANT4 v9.1 was used to propagate particles through the experimental set-up. The experimental hall was designed to be similar to that of the existing Modane Underground Laboratory (LSM), located at a minimum depth of about 1450 m or 4000 m w.e., with a size of 30 m (length) × 10 m (width) × 10 m (height). Fig. 1a shows the laboratory hall with Ge detectors surrounded by shielding. Fig. 1b shows the cryostat consisting of two copper vessels (inner vessel with a thickness of 0.5 cm and a mass of 139 kg, and an outer vessel with a thickness of 0.5 cm and a mass of 181 kg) containing about 100 kg of Ge supported by a copper plate with a thickness of 1 cm and a mass of 22 kg. The cryostat has a diameter of 67 cm and a height of 1.61 m. The crystals are arranged in 27 layers, each containing 12 crystals with a maximum diameter of 7 cm, a height of 2 cm and a mass of about 300 g each. The crystals (see Fig. 1c) are similar to those described in Ref. [15]. Total detector mass has been increased to about one tonne in the second round of simulations (see Section 5). The size of the cryostat has been increased too to hold the larger mass of target and cold electronics. Although we used the simplified design of a dark matter detector based on Ge target, it enabled us to estimate the background rates due to neutrons and gamma-rays from the most massive detector components and determine the requirements for passive shielding.

The statistical uncertainties of the simulation results reported here do not exceed 5%, being of the order of 1% for most reported configurations.

Table 2
Concentrations of natural uranium, thorium and potassium containing long-lived radioactive isotopes in LSM rock and concrete.

Element	U	Th	K
Rock	(0.84 ± 0.20) ppm	(2.45 ± 0.20) ppm	(6.8 ± 0.8) × 10^3 ppm
Concrete	(1.9 ± 0.2) ppm	(1.4 ± 0.2) ppm	(2.5 ± 0.4) × 10^3 ppm

3. Background from laboratory walls

The experimental hall in the model was similar to that of the existing Modane laboratory. It was surrounded by a 30 cm thick concrete layer. Gamma-rays and neutrons were generated evenly in a 30 cm thick layer of concrete and a 3 m thick layer of rock and emitted isotropically. The elemental compositions for rock and concrete were taken from Ref. [16] with small corrections based on recent analysis of the rock samples [13]. Despite differences in the composition and radioactive contamination, which can be found in Tables 1 and 2 respectively, the neutron spectra and absolute fluxes are similar for concrete and rock as shown in Fig. 2a. Consequently beyond 30 cm of concrete with radioactivity levels as measured in the existing Modane laboratory, the gamma-ray and neutron fluxes from concrete will largely dominate over those from rock (see Fig. 2b). It turns out that the 30 cm thick concrete layer contributes 96% to the total gamma-ray and electron fluxes beyond the shielding and 97% to the total neutron flux, so the rock fluxes can be neglected.

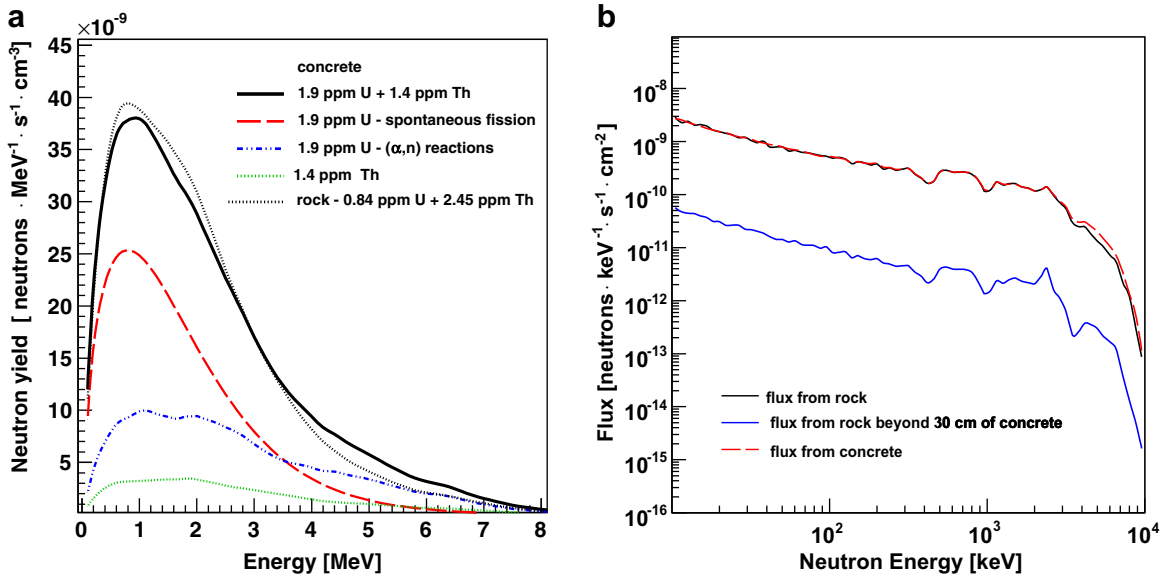

Fig. 2. (a) Energy spectra of neutrons from radioactivity in concrete (solid curve) and in rock (dotted curve) from SOURCES4A. Separate contributions from U (spontaneous fission and (α,n) reactions) and Th are also shown for concrete (see legend for details). (b) Neutron energy spectra from U and Th traces in rock at rock/concrete boundary (black solid curve) and concrete at concrete/air boundary (red dashed curve). The blue solid curve shows the neutron spectrum from rock at the concrete/air boundary. Details about compositions and contaminations are in Tables 1 and 2. The spectra are obtained by propagating neutrons from evenly distributed sources in rock/concrete, using GEANT4 v9.1, in the geometry set-up of Fig. 1a. (For interpretation of the references to colour in this figure legend, the reader is referred to the web version of this article.)

Some elements with high neutron capture cross-section may affect significantly neutron transport through rock or concrete. Since the capture cross-section rises with decreasing neutron energy, this will affect only low-energy neutrons which do not contribute to the nuclear recoil rate in dark matter detectors. The validity of the model for neutron transport through Modane rock and concrete was validated by the measurements of neutron flux in the laboratory [17].

3.1. Lead and hydrogenous shielding

Usually low radioactivity lead and copper are used to attenuate gamma-ray background from laboratory walls. Lead is preferred as shielding for gamma-rays because of its higher density and high Z. It was shown in Ref. [6] that 20–25 cm of lead can attenuate gamma-ray background by 5–6 orders of magnitude, depending on the energy. Two materials were considered for neutron shielding: polyethylene and water, both beyond 20 cm of lead.

Simulation results for background sources located outside the cryostat are summarised in Table 3; details on the background sources considered are also included. The first column reports the location of the radioactive sources considered along with their total mass and concentration of radioactive nuclides; the second column shows the shielding configurations (between the radiation source and the crystals); the electron and nuclear recoil event rates are given in columns three and four respectively. To quantify the detector sensitivity to the WIMP-signal, we present the results as a rate of single recoil events in the energy range 10–50 keV in a year, assuming a threshold of 10 keV for an energy deposition in any individual crystal. If for a primary neutron both single *n*-recoil and *e*-recoil were detected above the threshold, the event was rejected, since it will not be seen as a pure *n*-recoil due to the high discrimination power of the Ge detectors. No position sensitivity was assumed within a single crystal, and multiple scattering in a single crystal was considered as a single recoil event. If an event consists of an energy deposition of more than 10 keV in one crystal, accompanied by another deposition of less than 10 keV in a different crystal, then this event was treated as a single recoil. Event selection concerning gammas was performed using similar criteria as for neutrons, the only difference is the absence of *n*-recoils in gamma-ray induced events.

Table 3
Background event rate per year at 10–50 keV due to single nuclear/electron recoils from neutron/gamma interactions in 100 kg of Ge. Background sources are external to the cryostat.

Source	Shielding	e^--Recoil events	*n*-Recoil events
Concrete	20 cm Pb + 50 cm CH_2	–	0.064
1.9 ppm U, 1.4 ppm	20 cm Pb + 60 cm H_2O	–	0.125
Th, 2.5×10^3 ppm K	Cryostat in water 2 m/ 3 m	1.03×10^5/ 1300	–
Stainless steel (water container along the lab walls)			
121 tonnes, δ = 2 cm,	1 cm Cu (cryostat	8×10^5	17.2
1 ppb U/Th, 1 ppm K	vessels)		
Lead (outside the cryostat)			
3310 kg, δ = 20 cm, 1 ppb	50 cm CH_2 + 1 cm Cu	603	–
U/Th, 1 ppm K	(cryostat vessels)		
Polyethylene (outside cryostat)			
21 tonnes, δ = 50 cm,	1 cm Cu (cryostat	2.12×10^5	0.442
0.1 ppb U/Th,	vessels)		
0.1 ppm K			

δ = thickness.

Table 3 (first two rows, columns 3–4) shows that 50 cm of CH_2 or 60 cm of H_2O can attenuate the *n*-recoil event rate to a negligible level of $\ll$1 event per year. Polyethylene performs better due to its slightly higher fraction of hydrogen compared to water. Neutron fluxes from concrete, beyond different layers of polyethylene and water are shown in Fig. 3. Our results for CH_2 shielding agree with those reported previously in Refs. [7,13]. Our simulations were carried out with version 9.1 of GEANT4, whereas previous simulations were using an earlier GEANT4 version [7] and MCNPX [13].

3.2. Water shielding

Large-scale dark matter detectors will require significant investment. To reduce the cost of the experiment and optimise the shielding and active veto system, an option of having an instrumented water shield can be considered. Water is the cheapest material available for shielding and can be purified. Used in large quantities it can cope with both gamma and neutron backgrounds. This makes water very attractive as shielding. The construction of a new laboratory allows two options for water location: a water tank with the immersed cryostat or a layer of water along the lab walls. In the first case (see Fig. 4a) the cryostat is directly immersed in water; in the second case the water is contained in a stainless steel tank along the walls, as shown in Fig. 4b. Another advantage of using water is that it can be used as an active veto system, if instrumented with photomultiplier tubes (PMTs). PMTs will detect Cherenkov light produced by high-energy muons or secondary particles in muon-induced cascades. In this way an additional background rejection is provided by tagging muon-induced events in the veto in coincidence with a target signal.

We considered water as an alternative shielding against neutrons and gamma-rays. To shield the detector from gamma-rays will require a thickness of water well above the 60 cm needed for neutron background suppression (see Section 3.1). A thickness of 2–3 m of water was investigated in the set-ups shown in Fig. 4 – cryostat immersed in water or water along the laboratory walls held in a tank.

Fig. 5 shows the fluxes of gamma-rays and electrons (combined) coming from thorium in concrete, beyond different layers of water. Fig. 6 shows the spectra of single *e*-recoils in Ge beyond 3 m of water due to gamma-rays from U, Th and K in concrete, concentrations of Table 2 being assumed. The event rate is dominated by the contribution from thorium. More than 50% of events above 10 keV are single *e*-recoils. At 10–50 keV single *e*-recoils largely dominate the background rate.

Table 3 (third row) summarises the event rate due to single electron recoils at 10–50 keV initiated by photons coming from concrete beyond a 2–3 m thick water shield. Using 3 m of water, the sum of U, Th and K gives about 1300 events/year in 100 kg of Ge, requiring a discrimination factor of about 2×10^3 for their suppression. To achieve efficient attenuation, a thickness of 3 m of water is required, leading to a full size for a 100 kg scale experiment of more than 6.5 m in diameter and probably more than 7.5 m in height. A large-scale detector (1 tonne) may require a slightly thicker shield and bigger size for the full system, or better discrimination power, which is known to be achievable in cryogenic experiments [2,3]. The CDMS Collaboration has achieved with Ge detectors a discrimination factor of better than 10^4 against gamma-induced background and better than 10^6 against surface beta events [3]. Similarly the discrimination of Ge detectors in EDELWEISS-II was reported to be better than 10^5 against gammas and better than 10^4 against surface betas above the energy threshold of 15 keV [2].

Another option could be having water around the lab walls, contained in a stainless steel tank (Fig. 4b). The detector will be exposed to the background fluxes from the inner vessel of the water

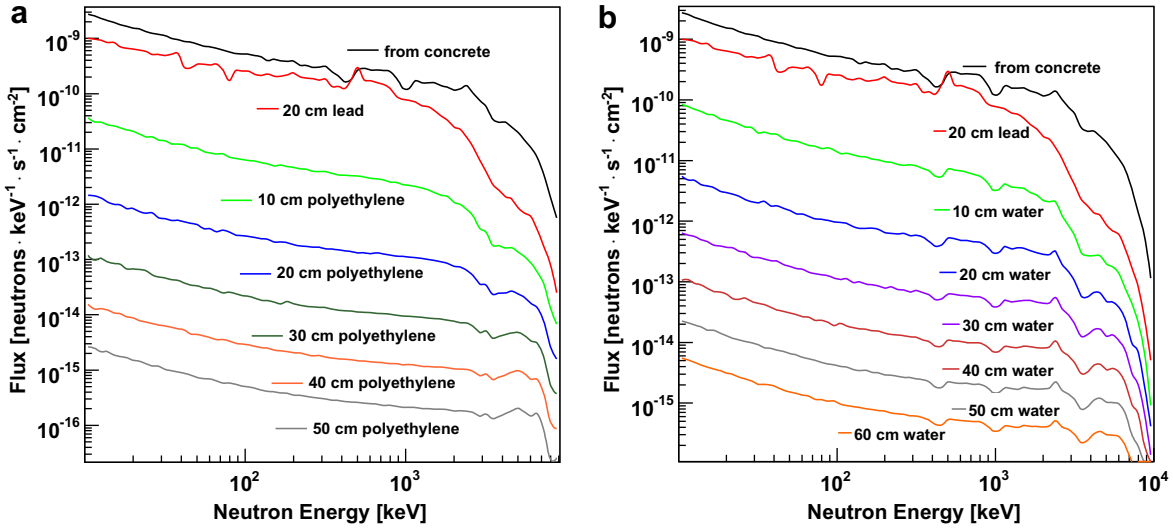

Fig. 3. Energy spectra of neutrons from 1.9 ppm of U and 1.4 ppm of Th in concrete beyond different thicknesses of polyethylene (a) and water (b).

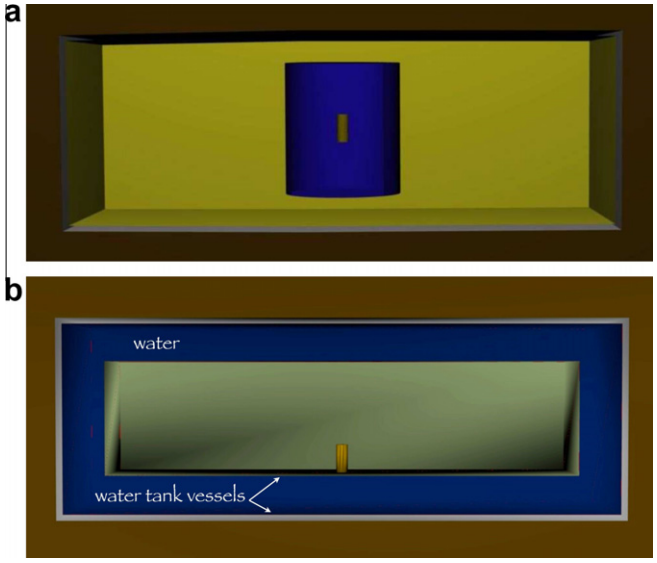

Fig. 4. View of the LSM laboratory from GEANT4 with water shielding the cryostat. Top: cryostat is immersed in water; bottom: water is in a stainless steel tank along the laboratory walls.

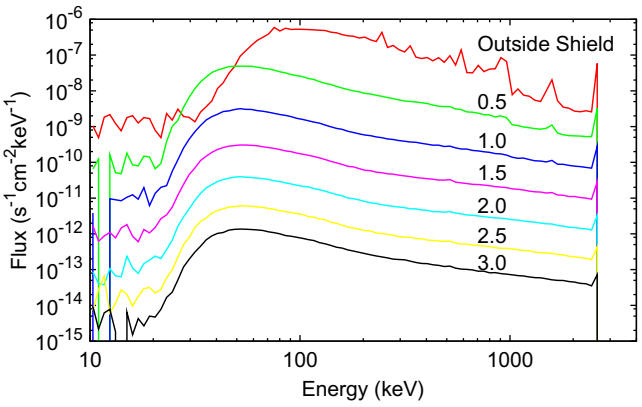

Fig. 5. Energy spectra of photons and electrons from 1 ppb of Th in concrete beyond different thicknesses of water shielding shown above the curves in meters.

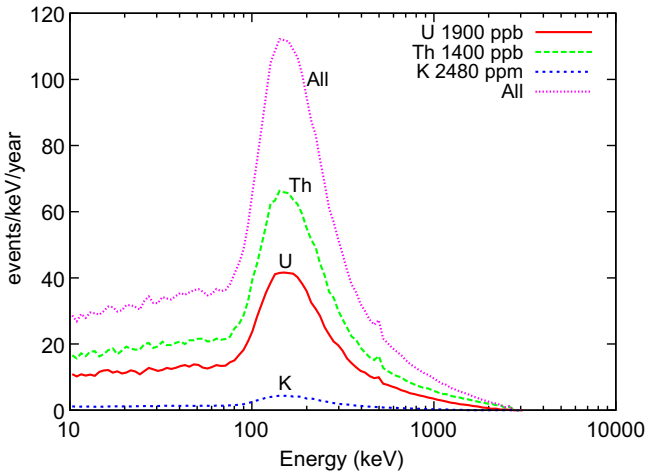

Fig. 6. Energy spectra of single *e*-recoils in 100 kg of Ge from concrete beyond 3 m of water shielding.

shield. The mass of the steel depends on the lab size and varies with the lab design. Assuming a thickness of 2 cm for the vessel, the total mass of steel is 121 tonnes. We assumed that the cryostat does not have any shielding from the radiation produced inside the lab hall. The benefit of this solution is an experimental hall free of any shielding and direct access to the detectors. The thickness of water should be similar to that found in the case of water tank around cryostat, but it turns out that the radiation from the inner vessel of the tank increases *e*-recoil rate to almost 10^6 events/year, while 17 nuclear recoils in a year of running are expected. To proceed with this set-up, extra shielding is necessary, as will be discussed in Section 4.2.

Fig. 7 shows the energy spectrum of single Ge recoils induced by neutrons from the uranium decay chain in the vessel of the water tank. To study the effect of the threshold the spectrum is plotted for an energy threshold of 5 keV rather than 10 keV as on the previous graphs. The event rate per year for an energy range of 10–50 keV is found to be 12.8 from U and 4.4 from Th decay chains. Decreasing the energy threshold to 5 keV increases the rate of single Ge recoils to 15.4 from U (20% increase).

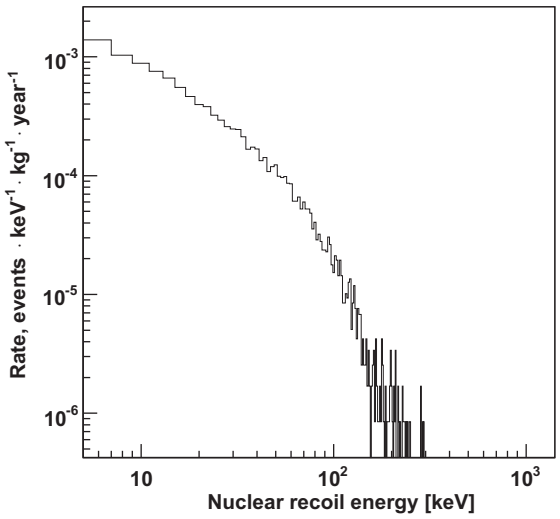

Fig. 7. Energy spectrum of single *n*-recoils in 100 kg of Ge from 1 ppb of uranium in the inner vessel of the water shield. An energy threshold of 5 keV was assumed to select events.

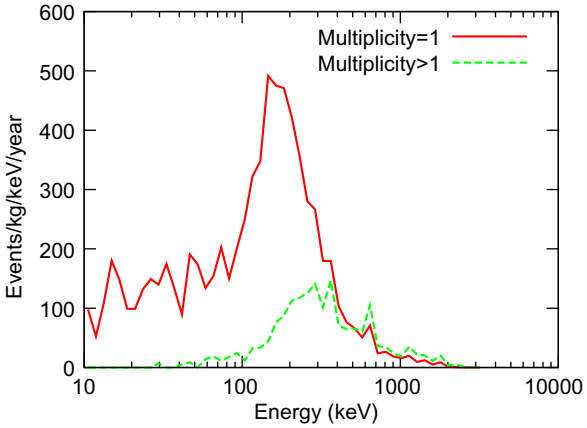

Fig. 8. Energy spectra of *e*-recoils in 100 kg of Ge from 1 ppb of uranium in the inner vessel (30.2 tonnes of stainless steel) of the water shield. For multiplicities more than 1, the energy threshold for individual crystals was set to 10 keV but the energy is counted as the sum of all energy depositions in all crystals.

Fig. 8 shows the energy spectra of single and multiple *e*-recoils induced by gamma-rays from the uranium decay chain in the vessel of the water tank. For multiple recoils the total energy deposited in an event is plotted on the horizontal axis. Reducing the energy threshold below 10 keV does not add much to the background event rate. The event rate for 1–50 keV range is about 12% higher than for 10–50 keV range.

4. Background from shielding and detector components

Shielding, as well as any detector components, produces background radiation that, if not sufficiently controlled, would affect the detector sensitivity. Only very pure materials should be placed close to the detectors. In the following sections some components of the shielding and the cryostat vessels are examined as radioactive background sources. Results are summarised in Tables 3 and 4. In the latter background sources are located within the cryostat. For some cases only neutron or gamma-ray background was simulated resulting in empty cells in the table. This was the case, for instance, for the gamma-ray background from rock, which was shown to be sufficiently suppressed by 20 cm of lead to achieve the required sensitivity for any large-scale detector [6]. Similarly, knowing that 60–70 cm of water attenuates the neutron flux down to the desired level, there was no need to simulate neutron transport through 2–3 metres of water. For some cases the simulation for specific geometry has not been done but an approximate result can be obtained by extrapolating similar simulations for slightly different geometry.

Without shielding the neutron and gamma-induced background rates would be $\sim 10^5$ and $\sim 10^9$ events per year, respectively.

Table 4
Background event rate per year at 10–50 keV due to single nuclear/electron recoils from neutron/gamma interactions in 100 kg of Ge. Background sources are detector components.

Source	Shielding	e^--Recoil events	*n*-Recoil events
Copper (cryostat) 320 kg, δ = 1 cm, 0.01 ppb U/Th, 10 ppb K	None	6677	0.0308
Stainless steel (inner cryostat vessel) 347 kg, δ = 0.5 cm, 1 ppb U/Th, 1 ppm K	None	4.04×10^5	2.54
	5 cm Pb + 10 cm CH_2	5.57×10^3	0.042
	10 cm CH_2 + 5 cm Cu	2.26×10^4	0.130
	10 cm $C_5O_2H_8$ + 5 cm Cu	–	0.521
Lead (inside the cryostat) 3310 kg, δ = 5 cm, 1 ppb U/Th	10 cm CH_2	-	0.557
Polyethylene (inside the cryostat) 366 kg, δ = 10 cm, 0.1 ppb U/Th, 0.1 ppm K	None	1.58×10^5	0.288
Polyethylene (inside the cryostat) 462 kg, δ = 10 cm, 0.1 ppb U/Th, 0.1 ppm K	5 cm Cu	1.38×10^4	0.333
Plexiglass (inside the cryostat) 592 kg, δ = 10 cm, 0.1 ppb U/Th	5 cm Cu	–	0.523

δ = thickness.

4.1. Metallic materials

Metallic materials are present in large quantities in any experimental set-up: in shielding or detector components (cryostat, holders, pipes, etc.).

Among them, lead, stainless steel and copper are the ones widely used in dark matter searches. Lead works as a very efficient shield against gamma background. Stainless steel and copper are usually used to build detector vessels. Lead and stainless steel are available with typical contamination levels of about 1 ppb for U and Th, and 1 ppm for K or slightly less. For copper these figures can be smaller by 2 orders of magnitude at least, electrolytic copper (quality NOSV from Norddeutsche Affinerie, Germany) [18,19] is available with a contamination level of <1.6 ppt for U, <5.6 ppt for Th and <2.8 ppb for K.

If a lead shield (20 cm thick) is placed to screen the detector together with polyethylene (see Section 3), it does not contribute to the background flux. Neutron background would be absorbed by the subsequent polyethylene shield; gamma background is mostly reabsorbed within the lead itself. Polyethylene and cryostat vessels (1 cm thick in total) also contribute to the suppression. This was confirmed by the simulations, see Table 3 (5th row).

An achievable purity level of 0.01 ppb or better for both U and Th makes copper the best material to be used close to the fiducial volume, as a material for a cryostat, for example. Neutron background from a copper cryostat was already simulated in

Ref. [11]. The results are also reported in Table 4 (1st row) together with the *e*-recoil event rate. Neutron recoil events should not limit the detector sensitivity to WIMPs, since less than 1 event per year at 10–50 keV is expected, while a discrimination factor of 10^4 is needed for *e*-recoils.

We also estimated possible contribution of ^{60}Co to the *e*-recoil rate. Assuming a concentration of 10 μBq/kg of ^{60}Co in the copper of the inner vessel [18], about 150 more *e*-recoils are expected per year. This does not add much to the results shown in Table 4 (first row).

Neutron interactions can produce multiple recoil events in a detector, whereas the WIMPs are expected to scatter only once. Therefore by looking at the multiplicity of interactions it is possible to reject some fraction of the neutron-induced background. Fig. 9a shows the multiplicity distribution of recoils (events with at least one nuclear recoil deposition were considered) from neutrons originating in the inner copper vessel of the cryostat with 0.01 ppb of U. If more than one energy deposition (with a threshold of 10 keV per crystal) due to either nuclear or electron recoils occured in different crystals, then an appropriate multiplicity was attributed to this event. If an energy deposition in a crystal was less than 10 keV, it was considered as undetected. As can be seen from Fig. 9a, 52% of events above 10 keV are expected to be single recoils. The effect of discrimination of single *n*-recoil events from multiple hit events (including *e*-recoils), can be seen from Fig. 9b. The solid curve shows events in which single *n*-recoils are the only depositions seen in the detector (multiplicity = 1). The dashed curve is the energy spectrum of nuclear recoils for events with multiplicity $\geqslant 1$. The total energy deposition from all *n*-recoils for each event is plotted. Fig. 9b shows a reduction of 35% of the event rate in the range 10–50 keV by means of multi-hit event rejection.

The multiplicity distribution of the events and hence, the rate of single *n*-recoils depends on the details of the set-up, for instance, on the distance between the crystals and the amount of other materials (copper) between them. Moving the crystals apart and adding more copper between them (as holders or additional shielding), results in a reduction of the total external background event rate but suppresses mainly multiple hit events leading in

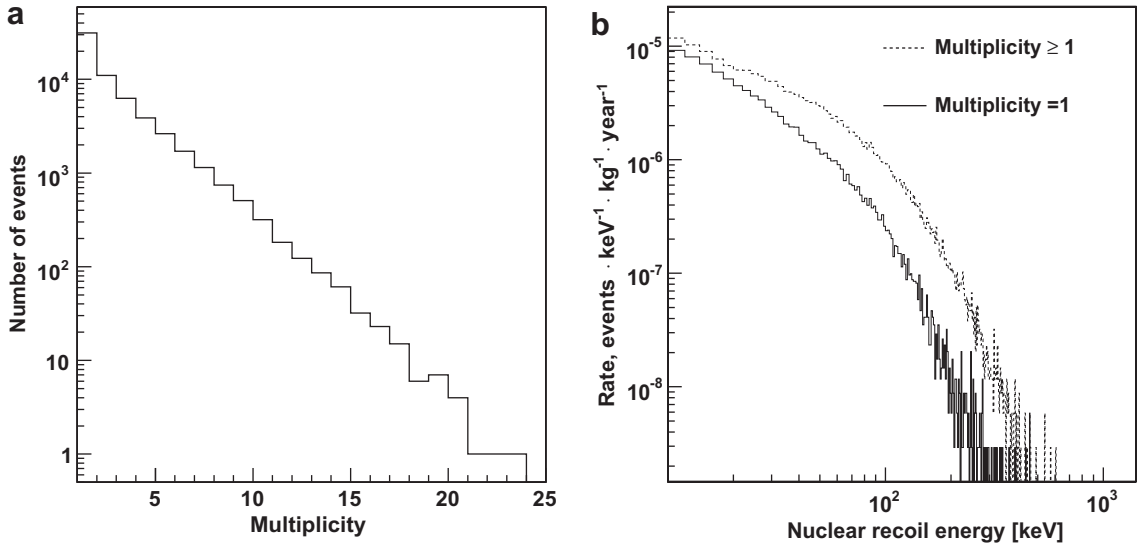

Fig. 9. (a) Multiplicity distribution of energy depositions due to nuclear recoils. (b) Solid curve – spectrum of energy depositions for single *n*-recoils events (multiplicity = 1), in 100 kg of Ge. Dashed curve – simulated spectrum for events with all multiplicities, the energy plotted is the total nuclear recoil energy deposited in each event (see text for more details). In both plots the inner cryostat vessel made out of copper (mass = 139 kg) was considered as the radioactive source. An energy threshold of 10 keV was assumed for a deposition in each individual crystal.

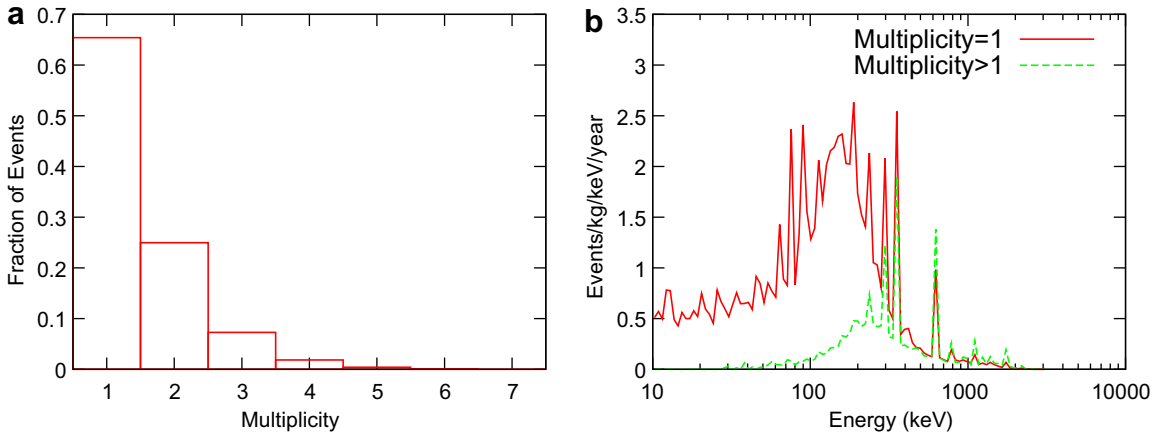

Fig. 10. (a) Multiplicity distribution of *e*-recoils in Ge above 1 keV from uranium in the copper inner vessel of the cryostat. (b) Energy spectra of electron recoils in Ge above 10 keV from 0.01 ppb of uranium in the copper inner vessel of the cryostat: single and multiple recoils are shown.

some cases (depending on the incident energy spectrum) to an even higher rate of single scatters, especially in outer crystals.

Fig. 10a shows the multiplicity distribution of *e*-recoils in Ge from 0.01 ppb of uranium in the inner vessel. Multiplicity is counted assuming an energy threshold of 10 keV for energy depositions in individual crystals. Fig. 10b shows the energy spectra of single and multiple *e*-recoils in Ge from 0.01 ppb of uranium in the inner copper vessel. Most events at 10–50 keV are single *e*-recoils.

Due to strength or other constraints, it may be necessary to use stainless steel in the construction of the cryostat or its internal parts. As an example, we assumed a different design for the cryostat, featuring an inner vessel in steel with a larger diameter. The cryostat was enlarged since shielding may be required to protect the crystals from radiation from stainless steel, regardless of its location (water tank of Fig. 4b or inner vessel of the cryostat). The simulation predicted $\sim 10^5$ *e*-recoils and 2.54 *n*-recoils in the detector due to the radiation from the inner vessel of the cryostat made out of stainless steel (see Table 4). Gamma-ray induced background can be reduced by 5 cm of lead, followed by 10 cm of polyethylene for neutron attenuation as reported in Table 4 (third row). However background from polyethylene needs to be examined as well. This will be covered in Section 4.2.

The factors that play an important role in the background production are the mass or thickness (for vessels) of the material and the distance to the target crystals. This can be seen when comparing two different background sources: the steel water tank (see Section 3.2) and the inner vessel of the cryostat also made out of stainless steel. If the two vessels have the same, relatively small ($\sim$1 cm), thickness, then the background event rates from neutrons or gamma-rays from both vessels are very similar despite large difference in masses. This can be explained by the fact that the large mass water tank vessel is located far away from the detector and the vast majority of neutrons and photons miss the target (small solid angle). The important parameter here is the thickness of the vessels which is assumed to be the same for both vessels.

4.2. Hydrogenous materials

Hydrogenous material, such as water, polyethylene and plexiglass, are commonly used as shielding against neutrons. The SNO collaboration reported a very low contamination level for heavy water (D_2O): $\sim 10^{-16}$ g U/Th cm^{-3} [20]. Water (H_2O) can be purified to a similar level giving only a very small contribution to the background rate. A higher background rate may come from polyethylene and plexiglass. We considered radiation coming from polyethylene and plexiglass assuming contamination levels of 0.1 ppb of U/Th and 0.1 ppm of K.

Shielding located inside the cryostat may help to attenuate background radiation coming from a material which is not very radio-pure if such a material is present in the experimental set-up. However, if lead and polyethylene in succession are used, gamma background arising from polyethylene itself produces a high rate of *e*-recoils in the detector (1.58×10^5 per year at 10–50 keV in 100 kg of Ge), while *n*-recoil rate is less than 0.3 per year (see Table 4, seventh row). To avoid a high *e*-recoil rate, the crystals need to be screened by a high-Z material, copper being preferred because of its high radio-purity. A reduction by one order of magnitude of the *e*-recoil rate due to the contamination of polyethylene was found when 5 cm of Cu are used (see Table 4, eighth row).

Similar suppression of gamma-ray radiation by Cu is expected if the source is located in the stainless steel vessel or any other materials and the low-Z shielding against neutrons is placed between the source and Cu (Table 4, fourth row). The background due to the copper shield itself can become dangerous if Cu is used in very large quantities: only contamination levels of <0.01 ppb of U/Th, <0.01 ppm of K and $\leqslant$10 μBq/kg of ^{60}Co can be safe.

Plexiglass could be an alternative to polyethylene. These two materials show a very similar performance as neutron background shielding (see last row of Table 4). The higher percentage of hydrogen in polyethylene explains the lower rates of single nuclear recoil events compared to plexiglass. Plexiglass, however, could be the best option in terms of radio-purity.

If there is a 50 cm thick layer of polyethylene outside the cryostat as a shield against neutrons (see Section 3.1), then less than 1 event per year from neutron-induced recoils is expected from 0.1 ppb of U/Th in polyethylene, while a high rate of *e*-recoils (2.12×10^5, see Table 3) is expected from gammas, possibly requiring additional Cu shielding.

5. Simulations for a tonne-scale target

The simulations for a simplified design of the cryostat described above were aimed at investigating the essential requirements for the shielding and its location, material selection and radio-purity. Based on the achieved conclusions, a new preliminary conceptual design for a tonne-scale EURECA experiment was developed [21]. The set-up includes two water tanks containing one cryostat each. The cryostat consists of seven concentric vessels with a total thickness of 2.1 cm of copper or more (in the bottom part) and contains either 506 kg of Ge crystals (28 copper plates or layers with 56 crystals each), or 253 kg of Ge and 288 kg of $CaWO_4$). If both targets were present, they were split evenly between the two cryostats. Each cryostat has an outer diameter of 1.28 m, a height of 1.86 m and the total mass of copper of 2.86 tonnes. We have completed the first round of simulations for this set-up with either 1012 kg of Ge, or 506 kg of Ge and 576 kg of $CaWO_4$ as a target.

The gamma-induced background from rock and concrete beyond 3 m of water in 506 kg of Ge and 576 kg of $CaWO_4$ was found to be only slightly higher (about 2×10^3 events/year at 10–50 keV) than for a $\sim$ 100 kg Ge target. This is due to (i) attenuation of the gamma-rays in thicker vessels of the water tank and the cryostat; (ii) smaller rate of electron recoils in $CaWO_4$ compared to the rate in Ge. As before, only single hit events have been included in the aforementioned rate.

Assuming 0.01 ppb of U/Th and 10 ppb of K, large mass copper vessels of the cryostat, copper plates and crystal holders (2.86 tonnes of Cu in total) can give a background event rate of electron recoils of about 1.9×10^5 events/year in 506 kg of Ge. The neutron-induced rate is found to be 1.6 events/year in 1012 kg of Ge and 1.2 events/year in 506 kg of Ge and 576 kg of $CaWO_4$. It is known that the best copper in terms of radio-purity has contamination levels smaller than one-half of the assumed values [18,19] that can result in a background event rate of the order of 1 event/year or less assuming a discrimination factor of 10^5.

The radio-purity of the target material of the future large mass dark matter detector needs to be kept below ppt levels for U/Th and ppb levels for natural potassium. Fig. 11 shows the energy spectra of events (electron recoils) in 506 kg of Ge (one cryostat) caused by intrinsic contamination of Ge crystals with 1 ppt of U/Th and 1 ppb of K. Secular equilibrium was assumed for the decay chains. When simulating intrinsic background we used the same approach as in Ref. [22]. Only events with energy deposition in one crystal exceeding 10 keV were counted. The numbers of events at 10–50 keV are 423 (U), 119 (Th) and 23 (K) per kg of Ge in a year of running. With a discrimination factor of 10^5, to keep the background rate below 1 event in a tonne of target per year in the region of interest, the crystal contaminations should not exceed 0.1 ppt of U/Th and 1 ppb of natural potassium. Neutron background from intrinsic crystal contamination can be rejected since spontaneous fission of uranium will be accompanied by energy depositions from fission products in the MeV range.

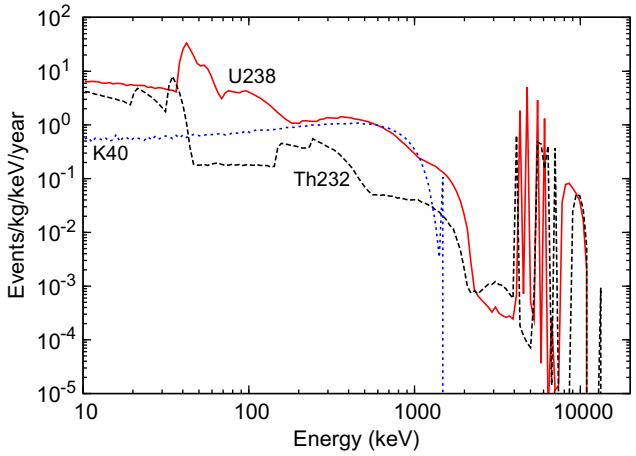

Fig. 11. Energy spectra of gamma-ray induced events in 506 kg of Ge (one cryostat) from intrinsic contamination of Ge with 1 ppt of U/Th and 1 ppb of K. Events with energy deposition in one crystal only are plotted.

The first simulations of muon-induced neutron background were carried out for the set-up described above assumed to be located at the LSM. Muons were transported from the surface down to the underground site and generated around the lab hall using the MUSIC and MUSUN codes [23–25]. Muons were passed to GEANT4 v9.2 [9] where the physics list suggested in Ref. [26] was used. All particles produced by muons passing through the rock, lab and the detector, were transported and their energy depositions in the water tanks and crystals were recorded. Details of these simulations have been reported [27–29] and will be published in a separate paper. We present here only the main results of the first simulation runs. 12 single nuclear recoil events were found at 10–50 keV in a 7.4 years of running of 1012 kg of Ge in two cryostats leading to a rate of 1.6 ± 0.5 events/year. All other events in the detector were found to be multiple hit events containing energy depositions from muons and all secondaries (gammas, electrons, neutrons and other hadrons) from muon-induced cascades. A similar rate was obtained for set-up with both Ge and $CaWO_4$ crystals but single nuclear recoil events were dominated by the high-energy oxygen recoils. This result does not assume any anti-coincidence between the events in the main target with energy depositions in the water tanks. If the water tanks are equipped with photomultiplier tubes and act as a water Cherenkov active veto system, then no events were observed in anti-coincidence between the target and the veto (with a veto threshold of 0.2 GeV) leading to an upper limit on the background event rate of 0.3 events/year in 1012 kg of Ge. This clearly shows that the muon-induced background is not a limiting factor for a tonne-scale detector located at LSM with a water Cherenkov veto system.

Simulations of neutron and gamma-ray backgrounds from other sources for a tonne-scale detector are in progress. Components with relatively small mass but potentially contaminated with radioactive isotopes (cables, feedthroughs etc.) need to be carefully analysed. Special attention should be paid to radon and its progeny. Cosmogenic activation of the crystals and detector components at the surface will also be investigated and material storage underground is foreseen.

6. Conclusions

Nowadays WIMP search demands high sensitivity detectors to explore the 10^{-9}–10^{-10} pb region, which requires practically the full suppression/discrimination of any background signal. Radiopurity of the materials, discrimination factor and cost are the main factors that affect background suppression. From the simulations presented in this paper several important conclusions can be drawn. It was shown that the background coming from the lab walls can be attenuated by 20 cm of lead along with 50/60 cm of polyethylene/water. A proper selection of concrete ingredients can reduce the background rate further, as we found background from concrete dominating over that from rock in the existing LSM laboratory.

Approximately 3 m of water can be used to attenuate both neutron and gamma-ray backgrounds. Two water shield configurations were examined: a whole experimental hall surrounded by water or the cryostat immersed in water. The hall surrounded by water requires a discrimination factor of 10^6 for gammas to remove the background from the steel tank (water tank), or additional inner shielding. The nuclear recoil rate from an electrolytic copper cryostat is much less than 1 event/year and does not require additional shielding even for a large-scale detector. A discrimination factor of 10^4 would suppress gamma-induced background from rock, concrete and copper in a 100 kg target. Better discrimination is required for a one tonne target mass inside a bigger cryostat. If a large mass of stainless steel is used in the cryostat construction, then additional background attenuation, to a level below 1 event/year, would require 5 cm of Cu inside 10 cm of CH_2 assuming a discrimination factor of about 10^4 and 100 kg target. Copper is available with high purity (< 0.01 ppb of U/Th, < 0.01 ppb of K and $\leqslant$10 μBq/kg of ^{60}Co) and should be used wherever possible instead of higher contaminated steel. More generally, no more than a few kg of stainless steel or other material with concentrations of about 1 ppb of U/Th are allowed near the detectors. All results in Tables 3 and 4 can easily be scaled to actual concentrations if needed. More materials and components for large-scale cryogenic detector construction with different targets will be studied in future.

Less than 0.3 single nuclear recoils per year are expected in one tonne of target from muon-induced neutrons in anti-coincidence with a water Cherenkov veto system.

From the simulations reported here it is obvious that low background and high discrimination power are essential for the performance of the EURECA experiment. The electron recoil discrimination factor of better than 10^5 and a background rate of 0.16 events/kg/day/keV at low energies, close to the required values, have recently been reported for Ge detectors in the EDELWEISS-II experiment [2,30].

Acknowledgments

This work has been supported by the ILIAS integrating activity (Contract No. RII3-CT-2004–506222) as part of the EU FP6 programme in Astroparticle Physics. One of us (VT) would like to thank ILIAS for the financial support of his Ph.D. research. We acknowledge also the support from the Science and Technology Facility Council (UK). We would like to thank the members of the EURECA Collaboration for fruitful discussions.

References

[1] R. Trotta, R.R. de Austri, L. Roszkowski, New Astron. Rev. 51 (2007) 316. <arXiv:astro-ph/0609126>.
[2] A. Broniatowski et al., Phys. Lett. B 681 (2009) 305. <arXiv:0905.0753> [astro-ph.IM].
[3] Z. Ahmed et al., CDMS Collaboration, Phys. Rev. Lett. 102 (2009) 011301.
[4] V.N. Lebedenko et al., Phys. Rev. D 80 (2009) 052010. <arXiv:0812.1150v1> [astro-ph].
[5] J. Angle et al., Phys. Rev. Lett. 100 (2008) 021303.
[6] M.J. Carson et al., Nucl. Instrum. Meth. A 548 (2005) 418.
[7] M.J. Carson et al., Astropart. Phys. 21 (2004) 667.
[8] H. Kraus et al., Nucl. Phys. B – Proc. Suppl. 173 (2007) 168.
[9] S. Agostinelli et al., GEANT4 Collaboration, Nucl. Instrum. Meth. A 506 (2003) 250.

[10] D. Budjas, L. Pandola, Gerda Report GSTR-07-010, 2007.;
L. Pandola, Private communication.
[11] V. Tomasello, V.A. Kudryavtsev, M. Robinson, Nucl. Instrum. Meth. A 595 (2008) 431.
[12] W.B. Wilson et al., SOURCES4A: a code for calculating (α,n), spontaneous fission, and delayed neutron sources and spectra, Technical Report LA-13639-MS, Los Alamos, 1999.
[13] R. Lemrani et al., Nucl. Instrum. Meth. A 560 (2006) 454.
[14] M. Herman, R. Capote, B. Carlson, P. Obložinský, M. Sin, A. Trkov, H. Wienke, V. Zerkin, EMPIRE: nuclear reaction model code system for data evaluation, Nucl. Data Sheets 108 (2007) 2655. <www.nndc.bnl.gov/empire219/downloads.html>. Empire 2.19 User's Guide.
[15] X.F. Navick, M. Chapellier, F. Deliot, S. Herve, L. Miramonti, Nucl. Instrum. Meth. A 444 (2000) 361.
[16] V. Chazal et al., Astropart. Phys. 9 (1998) 163.
[17] S. Fiorucci et al., Astropart. Phys. 28 (2007) 143.
[18] G. Heusser, Talk at LRT 2004. <http://lrt2004.snolab.ca>, 2004.
[19] M. Laubenstein et al., Appl. Radiat. Isot. 53 (2004) 167.
[20] T.C. Andersen et al., Nucl. Instrum. Meth. A 501 (2003) 399.
[21] H. Kraus, in: Talk at the 2nd LSM Extension Workshop, 16 October, 2009, Modane, France. <http://www-extension-lsm.in2p3.fr/workshop/EURECA-LSM.pdf>, 2009.
[22] V.A. Kudryavtsev, M. Robinson, N.J.C. Spooner, Astropart. Phys. 33 (2010) 91.
[23] P. Antonioli, C. Ghetti, E.V. Korolkova, V.A. Kudryavtsev, G. Sartorelli, Astropart. Phys. 7 (1997) 357.
[24] V.A. Kudryavtsev, N.J.C. Spooner, J.E. McMillan, Nucl. Instrum. Meth. A 505 (2003) 688.
[25] V.A. Kudryavtsev, Comput. Phys. Commun. 180 (2009) 339.
[26] A. Lindote, H.M. Araújo, V.A. Kudryavtsev, M. Robinson, Astropart. Phys. 31 (2009) 366.
[27] V.A. Kudryavtsev, Talk at the 2nd LSM Extension Workshop, 16 October, 2009, Modane, France. <http://www-extension-lsm.in2p3.fr/workshop/lsm-extension-workshop-vk.pdf>, 2009.
[28] V.A. Kudryavtsev, Talk at the WONDER-2010 Workshop, 22–23 March, 2010, LNGS-INFN, Italy. <http://wonder.lngs.infn.it/templates/wm_06_j15/download/kudryavtsev_lngs_mar10.pdf>, 2010.
[29] V. Tomasello, Ph.D. Thesis, University of Sheffield, 2009.
[30] E. Armengaud et al., arXiv:09120805v1 (astro-ph.CO).